Terrestrial laser scanner versus ground-based structure from motion photogrammetry for sinkhole characterization and monitoring in an urban area. A comparative assessment in the evaporite karst of Zaragoza city, NE Spain

Sevil-Aguareles, Jorge[1]; **Gutiérrez**, Francisco[1]; **Benito-Calvo**, Alfonso[2]

Sevil-Aguareles, J. (Corresponding author: jorgesevil@unizar.es) – ORCID: https://orcid.org/0000-0002-0068-4532

Gutiérrez, F. (fgutier@unizar.es) – ORCID: https://orcid.org/0000-0002-5407-940X

Benito-Calvo, A. (alfonso.benito@cenieh.es) – ORCID: https://orcid.org/0000-0002-6363-1753

[1] Departamento de Ciencias de la Tierra, Universidad de Zaragoza, Zaragoza, Spain

[2] CENIEH, Paseo Sierra de Atapuerca 3, Burgos, 09002 Spain

Abstract

Delimiting, characterizing, and monitoring active sinkholes in urban areas are fundamental steps for effectively managing the associated risks. These high-exposure scenarios require accurate data on hazard parameters (e.g., spatially-distributed subsidence rates), but the current investigation and monitoring techniques for sinkholes remain relatively undeveloped in comparison to other geological hazards, such as landslides. In this regard, we present the first comparative analysis of the performance of Terrestrial Laser Scanner (TLS) and ground-based Structure from Motion (SfM) photogrammetry for delimiting the actively deforming areas and characterizing the spatial patterns of ground displacement through the comparison of two pairs of high-resolution 3D point clouds. To assess their performance this work utilizes vertical displacement data measured by high-precision leveling. The main finding is that, despite TLS provides displacement data with less noise and internal distortion, the less expensive and easier-to-implement SfM photogrammetry using ground-based conventional cameras yields a comparable performance when accurate geodetic data is available. However, according to high-precision leveling data, both techniques may underestimate the extent and rate of the deformation, indicating that there is still the need to complement these high-resolution techniques with the use of high-precision methods such as leveling or additional geodetic benchmarks.

Keywords: sinkhole hazard, TLS, SfM, high-precision leveling, M3C2, subsidence rate

Introduction

The identification and contextualization of active sinkholes, the delimitation of the area affected by deformation, and the quantitative spatio-temporal characterization of ground displacement are key elements for sinkhole hazard assessment and risk management (Parise *et al.*, 2015; Gutiérrez, 2016; De Waele and Gutierrez, 2022). A thorough understanding of these elements is particularly important in the case of active sinkholes affecting urban areas, where they may cause significant social and economic damage, including the destruction of human structures and even fatalities. Numerous publications have reported on damaging sinkholes in urban areas worldwide, including the state of Florida, US (Waltham *et al.*, 2005; Jones and Blom, 2014; Gutiérrez, 2016), Maceió City, Brazil (Vassileva *et al.*, 2021), Guangxi region, China (Daoxian, 1988; Lei *et al.*, 2013), Gauteng Province, South Africa (Bezuidenhout and Enslin, 1970; Buttrick *et al.*, 2011; Theron *et al.*, 2017), Karapınar area, Türkiye (Dursun, 2022; Orhan *et al.*, 2023), Kuwait City, Kuwait (Goodings and Abdulla, 2002), Camaiore City (Buchignani *et al.*, 2008) and Quinis Village (Zini *et al.*, 2015), Italy, and the city of Zaragoza and its surroundings, in Spain, which is considered to be the area of the country where sinkhole activity has the greatest economic impact, making it one of the most dangerous areas in Europe in this regard (Gutiérrez *et al.*, 2008a).

Sinkholes occurring in this sector of northeastern Spain are commonly related to the rapid karstification of thick salt-bearing evaporitic bedrock mantled by alluvium (Gutiérrez *et al.*, 2007; Salvany *et al.*, 2007; Salvany, 2009). In addition to sinkhole activity affecting transportation infrastructure, agricultural areas, and industrial zones (Galve *et al.*, 2009; Desir *et al.*, 2018; Guerrero *et al.*, 2021; Sevil *et al.*, 2021), the city of Zaragoza itself experiences substantial sinkhole damage involving pavement repair (Carbonel *et al.*, 2015), the demolition of buildings (Sevil *et al.*, 2017), and the implementation of costly remediation programs with accumulated direct losses of the order of tens of million euro (Gutiérrez *et al.*, 2009; Anchuela *et al.*, 2012; Sevil *et al.*, 2020). The high exposure of vulnerable elements in urban areas, together with their intrinsic constraints, demands the development of specific sinkholes investigation and monitoring techniques, which are relatively undeveloped in comparison to other geological hazards such as landslides.

The main objective of this work is to compare and assess the performance of Terrestrial Laser Scanner (TLS) and close-range Structure from Motion (SfM) photogrammetry, with the assistance of high-precision leveling as control method, for delimiting the area affected by deformation and monitoring sinkhole activity in urban areas. These techniques are non-invasive investigation methods that have been successfully applied in the past to characterize and monitor the ground displacement associated with active sinkholes. High-precision leveling allows monitoring the vertical deformation related to sinkhole activity with the highest accuracy (submillimeter) and precision, but the measurements are restricted to the benchmarks installed on the surface (Kersten *et al.*, 2017; Sevil *et al.*, 2017, 2020; Desir *et al.*, 2018; Kobe *et al.*, 2019). TLS (Benito-Calvo *et al.*, 2018; Sevil *et al.*, 2021) and close-range SfM photogrammetry (Chakra *et al.*, 2019; Al-Halbouni *et al.*, 2022) can be used to model the terrain with high-resolution 3D point clouds of centimeter to millimeter accuracy. The comparison between consecutive point clouds allows resolving surface deformation related to sinkhole activity. The integration of high-precision leveling and TLS- or SfM-derived surface deformation models has proved to be a successful approach to address the aforementioned key sinkhole-related elements with hazard implications. This is achieved through the combination of a high-accuracy, low-resolution method with a lower-accuracy, very high-resolution investigation technique. However, this work explores two novel issues related to sinkhole monitoring in urban areas: (1) the performance of close-range SfM photogrammetry using a conventional ground-based camera, which is not affected by the restrictions that suffer the use of drones; and (2) the comparison of the performance of TLS and the more affordable SfM photogrammetry using a conventional ground-based camera.

Geological and geomorphological setting

The studied sinkhole, designated as the S. Lamberto sinkhole in this work, is located in the mantled evaporite karst developed in the central sector of the Ebro Cenozoic Basin, the southern foreland basin of the Pyrenees (NE Spain) (Fig. 1). This basin is longitudinally drained and dissected by the Ebro River, which in its middle reach has excavated an asymmetric valley into the Zaragoza Gypsum Formation, an Oligocene-Miocene evaporitic continental succession deposited in an extensive high-salinity playa-lake system (Quirantes, 1978). According to deep borehole data, this formation exceeds 850 m in thickness and its non-weathered zones mainly consists of halite (NaCl), glauberite ($Na_2Ca[SO_4]_2$) and anhydrite ($CaSO_4$) with intercalations of marls and mudstones. Only the upper part of the formation is exposed at the surface. In the near-surface weathered zones, the halite units have been dissolved and the glauberite and anhydrite beds have been transformed into secondary gypsum

($CaSO_4 \cdot 2H_2O$) by incongruent dissolution and hydration, respectively (Salvany *et al.*, 2007; Salvany, 2009; Gutiérrez *et al.*, 2023a). Because of the very high equilibrium solubilities of halite and glauberite (411 and 130 g/L; mass of dissolved solute in 1 L of solution; (De Waele and Gutierrez, 2022), their interstratal dissolution plays a major role in the development of damaging subsidence processes in the region and in Zaragoza city (Fig. 1) (Guerrero *et al.*, 2008, 2021; Galve *et al.*, 2009, 2015; Acero *et al.*, 2015; Gutiérrez *et al.*, 2015, 2018, 2019, 2023b; Benito-Calvo *et al.*, 2018; Desir *et al.*, 2018; Sevil *et al.*, 2021).

The asymmetric Ebro River valley displays a stepped sequence of terraces and pediments on the southern margin and a prominent gypsum escarpment along the opposite side. The S. Lamberto sinkhole lies on terrace T2 (first terrace above the floodplain), around 13 m above the valley floor (Fig. 1 and 2). Its altitudinal position (205 m a.s.l.) and data of a borehole drilled 3.4 km west of the studied sinkhole at 229 m a.s.l., suggest that the Quaternary alluvium at the sinkhole site is underlain by a dissolution residue and glauberite- and halite- bearing evaporitic bedrock (Salvany, 2009; Carbonel *et al.*, 2015). The fluvial terraces and pediments in this sector of the valley are pockmarked by large subsidence depressions and sinkholes, some experiencing very rapid subsidence (e.g., Benito-Calvo *et al.*, 2018; Desir *et al.*, 2018) and causing damage to man-made structures (Fig. 1b).

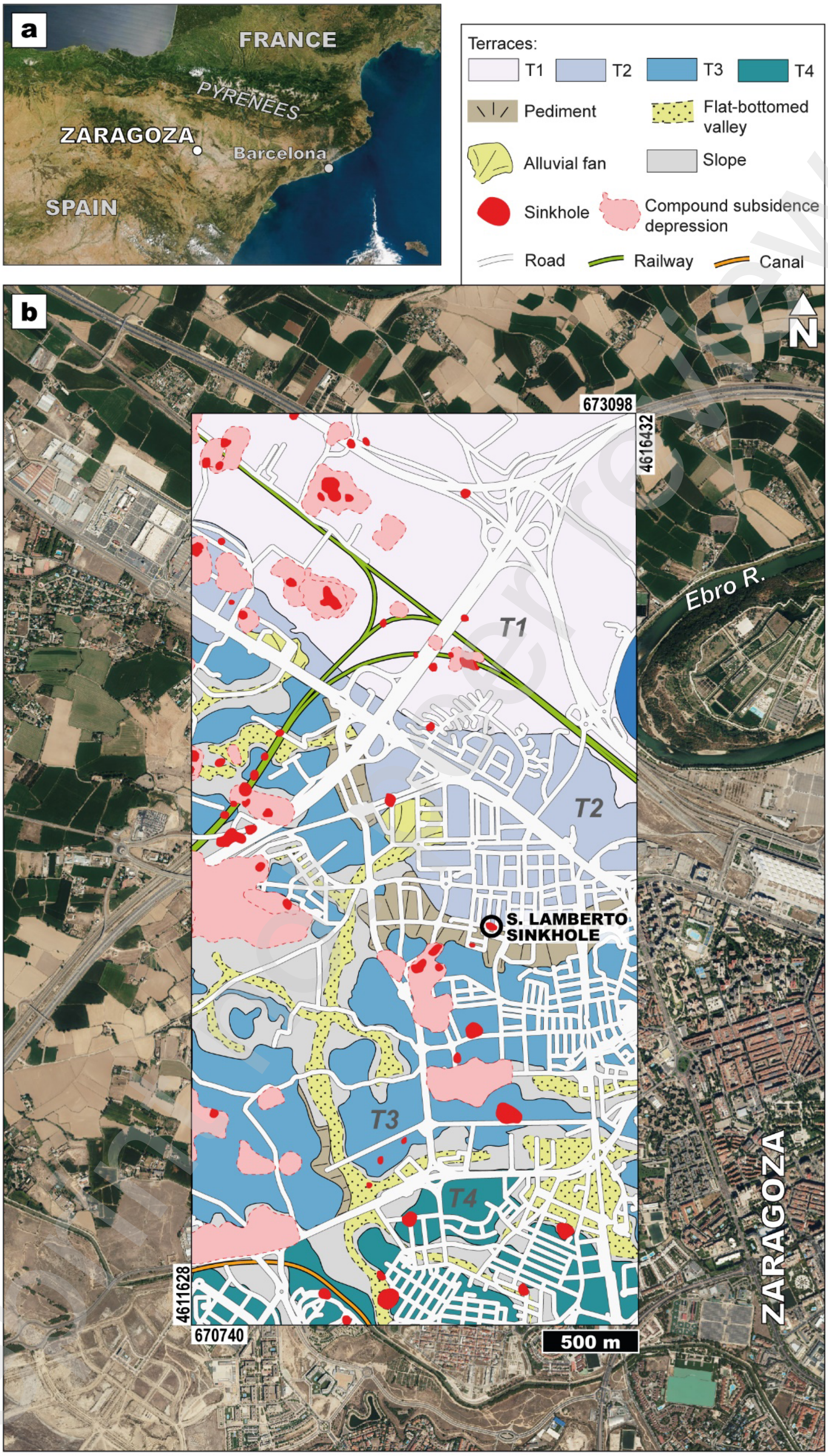

***Figure 1**. Geographic and geomorphological setting of the studied sinkhole (S. Lamberto sinkhole). (a) Location of Zaragoza city within the Ebro Cenozoic Basin south of the*

Pyrenees. (b) Geomorphological map showing the studied sinkhole and the spatial relationship between karst depressions and urban elements in the western sector of Zaragoza city (modified after Galve et al., 2009 and Sevil et al. 2020, 2021). Coordinate system: ETRS89 zone 30N.

Methodology

The first step in the study of the S. Lamberto sinkhole involved carrying out a detailed geomorphological map that allowed us to contextualize the investigated sinkhole (Fig. 1b and 2). Because it is located in an urbanized area of the western sector of Zaragoza city, we used aerial photographs from 1956 (American Flight B) printed at an approximate scale of 1:30.000 and a stereoscope to identify pre-existing geomorphologic features obliterated by decades of urban development.

Between June 2021 and June 2022, we surveyed the sinkhole by means of Terrestrial Laser Scanner (TLS) and ground-based Structure from Motion (SfM) photogrammetry. Both techniques were applied in the same area in order to analyze and compare their capability to resolve surface displacement through the comparison of 3D points clouds. We surveyed the sinkhole site with a Faro Focus 3D X330 TLS. Each survey comprised multiple partial scans that were registered into a single compound point cloud, with a mean registration error of 2.1 mm (Table 1), using the top-view-based placement and cloud-to-cloud tools of SCENE (2023). We followed this procedure, described in detail in Sevil et al. (2021), to reduce some initial distortion in the point clouds related to the spatially restricted positioning of the scanner along the Sánchez Rodríguez Street constrained by the presence of buildings. After this improved registration, we exported and joined the partial scans to produce a single point cloud for each TLS survey.

Additionally, we systematically took overlapping oblique photographs (.jpeg format) in June 2021 (875 images) and June 2022 (588 images) with a Canon EOS 5D Mark IV (full-frame CMOS sensor of 30.4 MP) and a Canon 16-35 mm lens (f/4L IS USM). The camera was mounted on a pole at 2.5 m above ground, with the line of sight at around 25° from the vertical, and the lens fixed at a focal depth of 35 mm. To assure the acquisition of good quality images, the photographs were taken with a wireless remote control, using the self-timer (2 sec), the stabilizer activated, high aperture (f/8-11), ISO 100, and a variable shutter speed, but always lower than the reciprocal of the focal depth (<1/35 sec). Subsequently, we used the software

Agisoft Metashape Professional (2022) to produce high-density 3D point clouds and high-resolution orthomosaics (ground sample distance of 0.56 and 0.51 mm for 2021 and 2022, respectively) and following the procedure typically applied in SfM photogrammetry using drone images (e.g., Westoby *et al.*, 2012; Micheletti *et al.*, 2015; Martínez-Fernández *et al.*, 2022). We installed 11 fixed ground control points (GCPs P0-P10, Fig. 2) to georeference the SfM-derived models. In order to obtain accurate coordinates, we employed a Leica TCRP1205 total station, plus a Leica DNA03 digital level to refine and update the vertical coordinates for each photogrammetric survey in such a subsiding context. For the latter procedure we installed two GCPs (Pcheck and P0 in Fig. 2) outside the sinkhole to verify that the reference point for refining and updating the vertical coordinates (P0) was in a stable area. We applied the same SfM processing parameters and GCPs distribution for both surveys to maintain consistency between models. The application of this procedure relied on the following assumptions: (1) the GCP P0 is located outside the subsidence area as revealed by previous leveling surveys; and (2) the GCPs needed for SfM photogrammetry are located within the subsidence area and experience vertical displacement maintaining constant horizontal coordinates. The distribution of these GCPs, located both inside and outside the sinkhole (Fig. 2), was determined on the basis of the surface deformation data provided by a high-precision leveling line previously installed along the street in November 2018, which is described below.

To assess the performance of TLS and ground-based SfM photogrammetry we used vertical displacement data measured along a 60-m-long high-precision leveling line installed in November 2018 along the Sánchez Rodríguez Street, traversing the S. Lamberto sinkhole, and with benchmarks (iron steel nails) spaced at 3 m (Fig. 2). This technique, employing a digital level (Leica DNA03) and a fixed-length bar-coded invar staff (Leica GPCL2), has been previously applied in sinkhole-related monitoring works (Kersten *et al.*, 2017; Sevil *et al.*, 2017, 2020, 2021; Desir *et al.*, 2018; Kobe *et al.*, 2019), providing the highest accuracy and precision (submillimeter) for vertical displacement. We produced a multitemporal cumulative vertical displacement plot (Fig. 4) with 13 leveling profiles measured between 3 and 6 months apart, from 18/10/2018 to 28/06/2022 (1349 days). We stationed the level at intermediate positions between benchmarks to take backsight and foresight measurements in fore and back runs, with values considered valid if the difference between readings was lower than 0.3 mm. This backward-forward method based on double leveling minimizes errors related to refraction and the displacement of the collimation axis (*ISO 17123-2*, 2001). This procedure allowed us to keep a vertical kilometer error below 4 mm/km.

To measure the distance (ground displacement) between each set of 3D point clouds (TLS and ground-based SfM photogrammetry), we used CloudCompare (2024) applying the following steps: (1) We subsampled the point clouds up to 10 mm to reduce processing times. (2) We cleaned, aligned, and cut all the point clouds to match the same extent. (3) We applied cloud-matching techniques between each set of point clouds. The point clouds obtained in June 2021 by each method served as reference clouds. Because of the procedure followed to generate the point clouds, they were already roughly aligned and it was only necessary to apply the automatic iterative closest point tool (ICP, Zhang, 1994) to improve their registration. (4) Subsequently, we conducted an initial M3C2 comparison to reduce the registration error between point clouds. Instead of manually clearing the point clouds to reduce the amount of noise related to changes in streets and buildings, as well as variations related to cars parked within the boundaries of the scanned area, we filtered them removing M3C2 distances higher than the mean subsidence rate measured by high-precision leveling over the June 2021-June 2022 period (-7.04 mm/yr). (5) Then, we conducted new ICP registrations between the reference point clouds (June 2021) and the filtered ones (June 2022). Following this procedure we were able to reduce the ICP registration errors from 7.3 to 5.0 mm, for the TLS-derived cloud, and from 9.4 to 6.3 mm for the SfM-derived one (Table 1). (6) We applied the transformation matrices of the second ICPs, which record the translation and rotation between point clouds, to the initial complete (i.e., unfiltered) clouds corresponding to June 2022 to improve their co-registration. (7) Finally, we measured the Multiscale Model-to-Model Cloud Comparison (M3C2) distance between the initial reference point clouds (June 2021) and the improved-registration clouds (June 2022) to measure the surface displacement related to the activity of the S. Lamberto sinkhole.

A comprehensive description of the M3C2 algorithm is presented in Lague et al. (2013). In summary, it measures the mean 3D distance between point clouds considering surface normals within a radius consistent with the local surface roughness. Additionally, the algorithm determines a local confidence interval that takes into account the surface roughness of the clouds, their position uncertainty, and their registration error (Lague *et al.*, 2013). In this study we applied the M3C2 algorithm in standard mode for both sets of point clouds, using a diameter of 20 cm for the normal and projection scales, and a maximum investigation depth of 4.6 cm. The latter value is twice the maximum vertical displacement measured by high-precision leveling in the sinkhole between June 2021 and June 2022. M3C2 distances larger than the maximum depth were discarded. For estimating the final registration error we used average values computed between: (1) the mean SCENE compound point cloud and the filtered ICP registration errors for the TLS-derived M3C2 displacement model; and (2) the Agisoft Metashape Professional vertical error of the point clouds and the filtered ICP error of the SfM-derived M3C2 displacement model (Table 1). Finally, we used both QGIS (QGIS.org, 2023) and R (R Core Team, 2022) in combination to analyze and compare the M3C2 displacement models and the high-precision leveling data. The latter vertical displacement data, with utmost accuracy, was used to assess and compare the performance of the two ground-based methods (TLS and SfM photogrammetry) for sinkhole monitoring in an urban area.

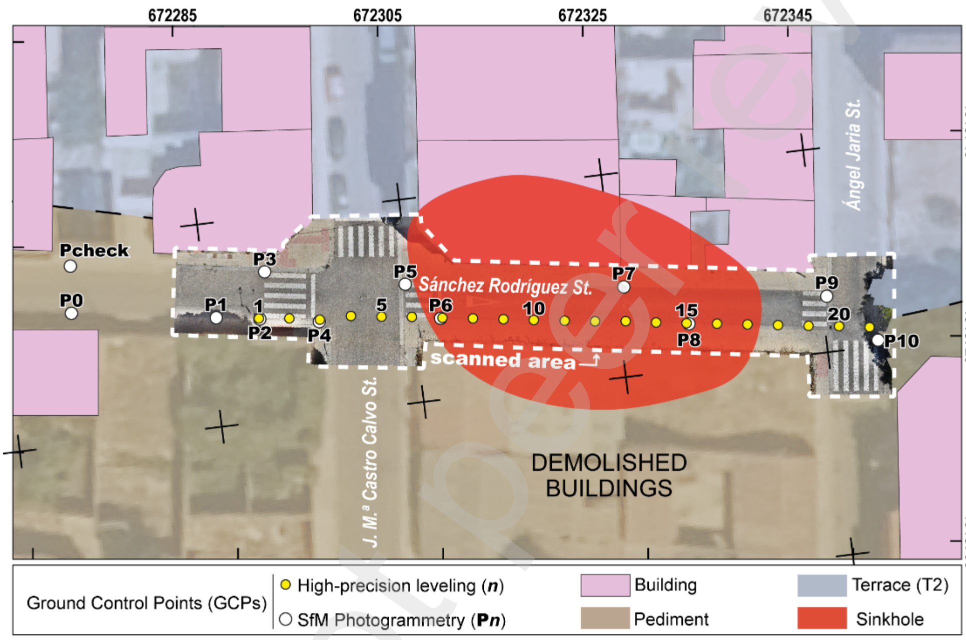

Figure 2. *Detailed map of the Sánchez Rodríguez Street displaying the spatial distribution of geomorphic and urban features, the scanned area, and the position of the ground control points used for high-precision leveling and ground-based SfM photogrammetry. The delineation of the sinkhole perimeter is based on the stereoscopic interpretation of aerial photographs from 1956 printed at a scale of 1:30,000. Coordinate system: ETRS89 zone 30N*

Point cloud origin	**TLS**		**SfM**	
Point cloud date	18/06/2021	16/06/2022	09/06/2021	28/06/2022
Number of points	14,058,546	8,876,769	18,329,975	16,787,553
SCENE mean compound point cloud registration error	2.1		*NA*	
Agisoft XY error	*NA*		*10.7*	*5.0*
Agisoft Z error	*NA*		6.0	5.1

RMS unfiltered ICP	*Reference cloud*	7.3	*Reference cloud*	9.4
RMS filtered ICP		5.0		6.3
Mean error		3.5		5.8

Table 1. *TLS- and SfM-derived point cloud data and registration errors (mm).*

Results

According to the geomorphological map interpreted using aerial photographs from 1956 (Fig. 1), the S. Lamberto sinkhole had an approximate area of 610 m^2 and a major axis 36 m long with a WNW-ESE orientation (115º azimuth). The georeferencing of this map over the most recent orthoimages (PNOA Spanish National Geographic Institute) shows that the investigated sinkhole affects a street, several residential buildings and an industrial warehouse now demolished (Figs. 2 and 3). Surface deformation related to the sinkhole activity was evident in the sidewalks and carriageway until sometime between June 2013 and August 2014, when the street was resurfaced (Fig. 3). Prior to this pavement repair, the sinkhole used to display a symmetric sag 25 m long in the street. Nowadays, after the maintenance works, no distinct deformation features ascribable to the sinkhole have developed yet (e.g., cracks, scarps, flexures), and the only clear evidence of its subsidence activity is the existence of cracks in the buildings and the formation of a small puddle in the deepest part of the subsidence depression after rainfall.

Figure 3. *Evolution of the study area between (a) 21 March 2013 and (b) 11 May 2024.*

The 60 m long leveling line installed along the street shows a section at least ≥57 m-long, between benchmarks 2 and 21, that is affected by subsidence operating at rather constant rates (Fig. 4 and Table 2). Note that active subsidence extends into a non-accessible area beyond the eastern tip of the line (benchmark 21). The 13 cumulative vertical displacement profiles gathered over the monitoring period (3.7 yr) indicate mean and maximum (benchmark 11) subsidence rates of 6.1 and 17.9 mm/yr, respectively. The section that records active deformation can be divided into three different segments: (1) A western slowly subsiding section 18 m long, between benchmarks 1 and 7, with mean and maximum subsidence rates of 1.4 and 2.7 mm/yr, respectively. (2) A rapidly subsiding sector 24 m long, between benchmarks 8 and 15, which is spatially consistent with the extent of the sinkhole interpreted using the aerial photographs. The mean and maximum subsidence rates measured in this segment were 10.7 and 17.9 mm/yr, respectively. (3) A segment 18 m long, between benchmarks 16 and 21, that records settlement related to an adjoining sinkhole, which was not identified in the geomorphological map, nor in the initial onsite inspection. We are not able to identify the limits of this active sinkhole because of the existence of a wall between the Sánchez Rodríguez St. and the adjacent undeveloped plot (Fig. 2). The mean and maximum subsidence rates measured in this segment were 4.7 and 7.2 mm/yr, respectively. Most likely more rapid subsidence operates to the east, beyond the leveling line. Regarding the temporal evolution of subsidence rates measured by high-precision leveling, the S. Lamberto sinkhole experienced slightly faster subsidence (mean and maximum rates) during the first 20 months of the monitoring period, until May 26, 2020, with average mean a maximum rates of -8.7 and -22.8 mm/yr, respectively. During the remaining 25 months of the leveling period, of which 12 months overlapped with the TLS and the close-range SfM photogrammetry surveys, the studied sinkhole experienced slightly slower average mean and maximum rates of -6.1 and -16.5 mm/yr, respectively (Table 2).

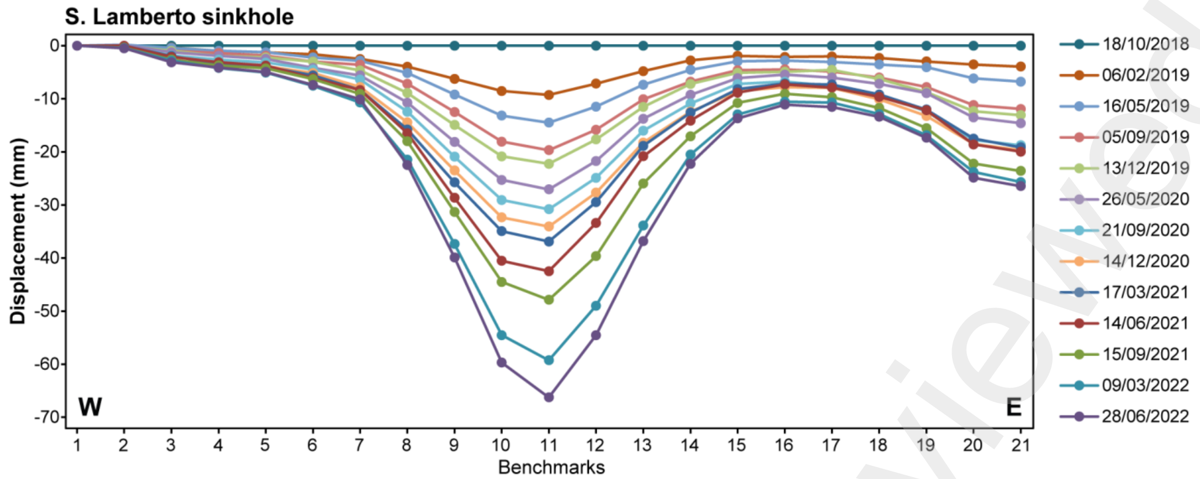

Figure 4. *Cumulative vertical displacement profiles generated from the high-precision leveling data gathered along the Sánchez Rodríguez Street between 18 November 2018 and 28 June 2022. The greater spacing between the leveling profiles of September 2021 (green) and March 2022 (blue) is not related to an increase in the subsidence rate, but to a longer time span between surveys.*

S. Lamberto sinkhole													
Measurement dates	18/10/2018	06/02/2019	16/05/2019	05/09/2019	13/12/2019	26/05/2020	21/09/2020	14/12/2020	17/03/2021	14/06/2021	15/09/2021	09/03/2022	28/06/2022
Mean kilometric error (mm/km)	1.785												
Length of line/points	60/21												
Length affected by subsidence (m)		60-57	57	60-57	60-57	57	60-57	60-57	57	60-57	60-57	60-57	60-57
Leveling points with subsidence		20	19	20	20	19	20	20	19	20	20	20	20
Measurement period (days)		111	210	322	421	586	704	788	881	970	1063	1238	1349
Mean cumulative subsidence (mm)		-3.4	-5.4	-7.6	-8.6	-10.7	-12.2	-13.5	-14.6	-15.2	-17.7	-21.0	-22.5
Maximum cumulative subsidence (mm)		-9.3	-14.5	-19.7	-22.3	-27.1	-30.8	-34.1	-36.9	-42.5	-47.9	-59.3	-66.3
Mean subsidence rate (mm/yr)		-11.2	-9.4	-8.6	-7.4	-6.7	-6.3	-6.3	-6.1	-5.7	-6.1	-6.2	-6.1
Maximum subsidence rate (mm/yr)		-30.5	-25.2	-22.3	-19.3	-16.9	-16.0	-15.8	-15.3	-16.0	-16.4	-17.5	-17.9

Table 2. *Summary of the high-precision leveling data gathered across the S. Lamberto sinkhole.*

The two TLS scans (June 18, 2021-June 16, 2022) and the two photogrammetric surveys (June 9, 2021-June 28, 2022) covered roughly coincident time spans, 0.99 and 1.05 years long, respectively. Table 1 includes acquisition dates of the point clouds, their size, and the resulting errors after the different registration processes. The comparison between the first and the second point cloud of each set using the M3C2 algorithm allowed us to produce two vertical displacement models of the sinkhole site for almost the same period but using two different techniques (Fig. 5). This enables a comparison of the performance of TLS and ground-based SfM photogrammetry in an urban area to accurately delimit the area affected by deformation and assess quantitatively its magnitude with a very high spatial resolution.

The TLS-derived M3C2 displacement data display a normal frequency distribution (mean: -0.4 mm, range: -66.1 – 75.1 mm, median: -0.4 mm, interquartile range (IQR): -1.3 – 1.0 mm) and the 3D displacement model shows a semicircular area in the central sector of the street, clearly affected by subsidence, which is spatially consistent with the location of the S. Lamberto sinkhole identified by the interpretation of old aerial photographs and the on-site inspection (Fig 5a). We have no data to the south in this area due to the existence of a building in the initial scan. This model reveals subtle uplift between the subsidence area and the wall of the residential building on the opposite side of the street, that might be related to the deflection of the bending stresses experienced by the rigid tiles of the northern sidewalk (e.g., Desir *et al.*, 2018; Sevil *et al.*, 2020). Additionally, the M3C2 model displays isolated points with large displacement values on its boundary. We interpret these outliers as noise resulting from the lack of coherence between the point clouds due to the modification of the surroundings, such as building demolition, vegetation movement, and changes in parked vehicles. Despite this, the clearly identifiable subcircular subsidence sector has a length of 21 m and an area of 97 m^2. The subsiding area with statistically significant change at a confidence interval of 95% covers a smaller area (13 m across and 29 m^2, Fig. 5b). Regarding the points with statistically significant change which location is consistent with that of the sinkhole, the median and maximum subsidence rates are 10.3 and 18.7 mm/yr, respectively. The described outliers also record statistically significant displacement values because of their high magnitude but have not been included in the analysis.

The SfM-derived M3C2 displacement data displays a normal frequency distribution with a slight negative skewness (mean: -1.3 mm, range: -76.3 – 76.1 mm, median: -0.1 mm, IQR: -6.3 – 4.2 mm, skewness: -0.6) and the 3D displacement model shows a subcircular area affected by subsidence in the central sector of the street (Fig. 5c). Its location is spatially consistent with that of the S. Lamberto sinkhole identified in the aerial photographs, albeit with a smaller area as in the TLS-derived model. The subsidence zone is surrounded by areas that according to the M3C2 displacement model undergo uplift. Additionally, the model displays two apparent subsidence areas at the NW and SE corners with the highest deformation rates. Although the position of the central sector affected by subsidence matches with the studied sinkhole, the distribution of the surrounding areas affected by uplift and subsidence, together with their displacement magnitude, seem to indicate that the model has undergone some artificial distortion during the photogrammetric processing. Additionally, as in the TLS-derived M3C2 displacement model, there are outliers related to the lack of coherence between the consecutive 3D point clouds attributable to changes non-related to the sinkhole activity. Despite the potential artificial distortion and the noise, the SfM-derived M3C2 displacement model allows identifying a subcircular area affected by subsidence with a length of 17 m and an area of 81 m^2, with only a small fraction showing statistically significant change at a confidence interval of 95% (Fig. 5d). According to the SfM-derived model, this sector experienced median and maximum subsidence rates of 11.6 and 38.3 mm/yr, respectively.

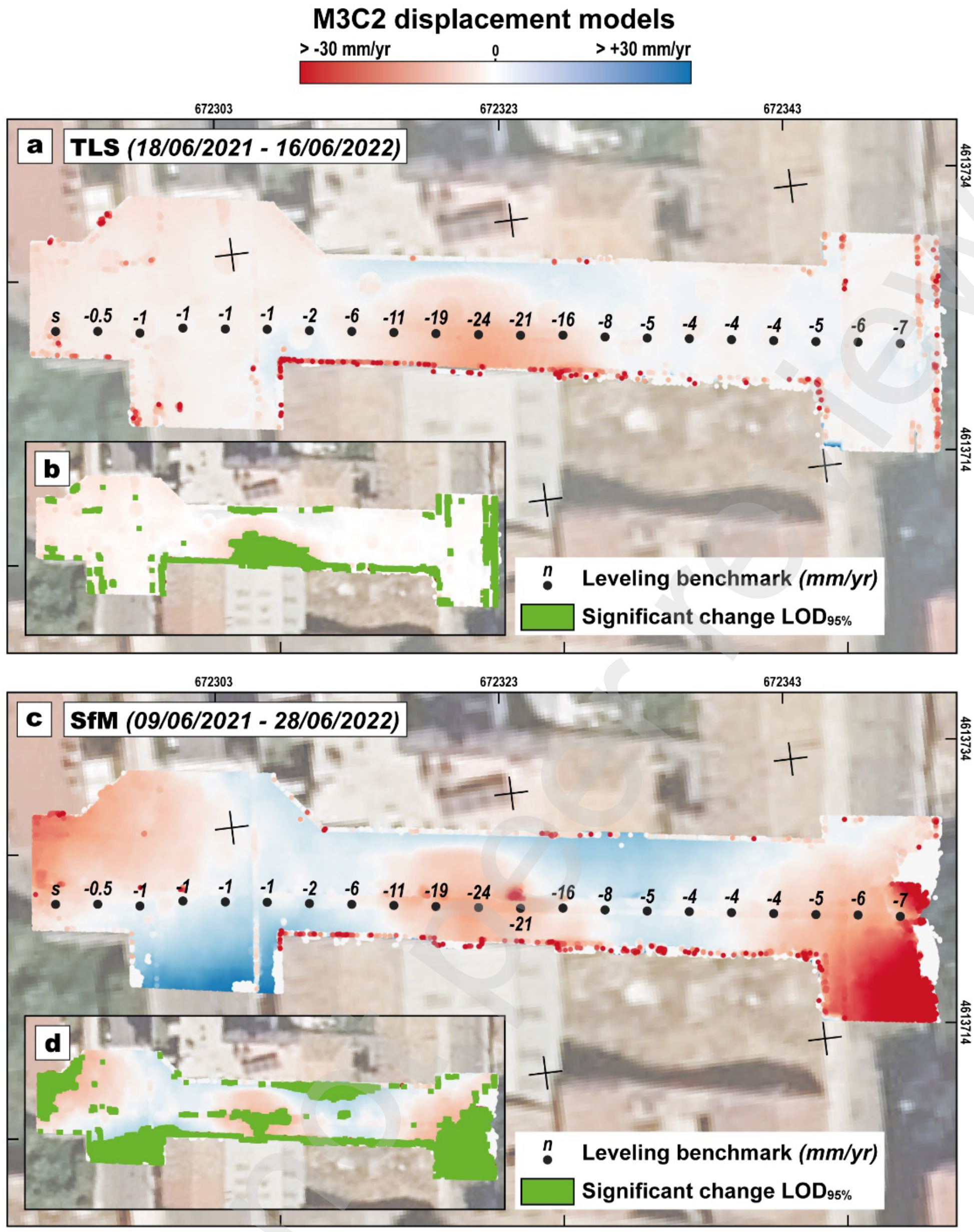

Figure 5. *M3C2 displacements models produced from the TLS (a) and ground-based SfM photogrammetry (c) data gathered in the study area between June 2021 and 2022, and areas where the surface displacement (b and d) can be considered as statistically significant with a confidence threshold of 95%. The figure includes the identification of the benchmarks used for high-precision leveling and the deformation rates in mm/yr measured at each one between June 2021 and 2022. The 's' identifies the point of origin of the leveling profiles. Coordinate system: ETRS89 zone 30N*

Discussion

As shown in the scientific literature, TLS (Benito-Calvo *et al.*, 2018; Sevil *et al.*, 2021) and close-range SfM photogrammetry (Al-Halbouni *et al.*, 2017; Petschko *et al.*, 2022) are suitable techniques for investigating the activity of sinkholes with high spatial resolution and accuracy through the comparison of consecutive high-resolution surface data (e.g., 3D point clouds, Digital Surface Models). Some features of these techniques make them particularly suitable for urban areas, including their non-invasive nature, relative quick and flexible data collection (no need for traffic interruption), and the straightforward installation of benchmarks, if needed (Sevil *et al.*, 2021). TLS and close-range SfM photogrammetry have been successfully applied in the past but, to date, no scientific work has comparatively assessed their performance to: (1) delimit the area affected by deformation; and (2) determine the magnitude and spatial patterns of surface displacement. In order to have independent vertical displacement data for the assessment of the two techniques, this work included the monitoring of the sinkhole by means of high-precision leveling. Despite its restricted spatial resolution, this technique has proved to be able to provide vertical displacement measurements with the highest accuracy and precision (Kersten *et al.*, 2017; Sevil *et al.*, 2017, 2020, 2021; Desir *et al.*, 2018; Gutiérrez *et al.*, 2019; Kobe *et al.*, 2019).

According to all the information gathered during the present investigation, the S. Lamberto sinkhole can be classified as an active cover-sagging sinkhole, following the genetic classification proposed by Gutiérrez et al. (2008b). During the leveling period (October 2018 - June 2022) it has experienced stationary and progressive subsidence. Mean and maximum subsidence rates display an initial slowdown period (October 2018 – May 2020), followed by the stabilization of the subsidence rates, including the period of the TLS and SfM surveys. It is important to note that the recorded continuous sagging subsidence does not allow ruling out a potential collapse event. Previous investigation in the same sector of the city of Zaragoza have identified collapse (e.g., Sevil *et al.*, 2017) and sagging-collapse sinkholes (e.g., Carbonel *et al.*, 2014, 2015).

Geomorphological mapping through the stereoscopic interpretation of aerial photographs from 1956 served to identify the S. Lamberto sinkhole, understand its context, and roughly estimate an area affected by deformation of 610 m^2 with a major axis of 36 m. Regarding the size and limits of the sinkhole, high-precision leveling provided the most accurate information, although restricted to the leveling line, with a section at least 60 m long affected by subsidence. This section comprises three different segments: an inner sector 24 m long experiencing faster subsidence surrounded by slower segments of 18 m long to the west and at least 18 m to the east. This eastern subsiding segment corresponds to an additional adjoining subsidence structure not identified in the initial geomorphological map. The M3C2 displacement models obtained through the comparison of 3D point clouds gathered by TLS and close-range SfM photogrammetry display a smaller area affected by active deformation, covering 97 and 81 m^2, and with major axes 21 m and 17 m long, respectively. These subsidence areas essentially coincide with the section of the leveling line affected by relatively fast subsidence. However, neither the M3C2 models nor the interpretation of low-resolution aerial photographs allowed the identification of the slow-subsidence aureoles detected by high-precision leveling. The underestimation of the extent affected by subsidence based on geomorphological mapping using conventional data compared to the results of other more precise site investigation techniques, such as leveling, photogrammetry or trenching has been illustrated in the scientific literature (Al-Halbouni *et al.*, 2017; Desir *et al.*, 2018; Gutiérrez *et al.*, 2018; Menezes *et al.*, 2020; Sevil *et al.*, 2020). The underestimation of the subsidence area from the M3C2 displacement models, that only detect the faster and most hazardous subsiding zone, compared to leveling data can be attributed to the lower precision and accuracy of TLS and SfM photogrammetry compared to leveling (e.g., Sevil *et al.*, 2021). Thus, the detection of the slow-subsidence zones by TLS and SfM photogrammetry would require longer monitoring periods.

High-precision leveling served to monitor vertical displacement with the highest accuracy, even detecting surface deformation in the western sector of the sinkhole despite its very slow subsidence rates (≤ 1 mm/yr, Fig. 4 and 5). As mentioned before, this technique suffers from limitations related to the restricted spatial resolution of the data and the potential loss of benchmarks during long monitoring periods. Still, regarding the last constraint, the installation of the benchmarks in accessible areas considering the street dynamics, such as the vehicle passing areas, the location of dumpsters, and the layout of parking spaces, allowed us to monitor the sinkhole over 3.7 years without losing any control point despite the demolition of the adjacent buildings Previous works have shown the usefulness of high-precision leveling for identifying sinkhole boundaries (e.g., Desir *et al.*, 2018). However, in the present investigation the whole leveling line most probably has experienced subsidence, (the start point is assumed to be stable; 's' in Fig. 5), and therefore it is not possible to identify the sinkhole edge with absolute certainty and the measured vertical displacements and rates should be considered as minimum values. Nevertheless, the fact that between November 2018 and June 2022 (3.7 yr) the high-precision leveling benchmark 2 only recorded a cumulative subsidence of 0.5 mm seems to indicate that such edge is very near and that the deviation between the measurements and the actual values is negligible. This is a common limitation when dealing with sagging sinkholes typical of evaporitic terrains, which are characterized by slow-moving marginal areas (De Waele and Gutierrez, 2022), for which it is advisable to install much longer leveling profiles while maintaining a relatively short spacing between benchmarks, even though this would substantially increase the time needed to measure the profile.

The two M3C2 displacement models generated from two pairs of 3D point clouds taken one year apart by TLS and close-range SfM photogrammetry detected an area affected by subsidence with very similar spatial distribution (Fig. 5), similar size (97 m^2 for TLS versus 81 m^2 for SfM), and with comparable median subsidence rates of 10.3 mm/yr (TLS) and 11.6 mm/yr (SfM). This means that the more affordable and easier-to-implement close-range SfM photogrammetric method, assisted with geodetic measurements including high-precision leveling, is able to detect and monitor an active sinkhole in an urban area with results comparable to those obtained using TLS, a technique that requires a much more expensive and delicate measuring equipment. Nevertheless, it is important to note that the TLS-derived M3C2 displacement model showed substantially lower noise, probably due the capability of the TLS to obtain 3D point clouds with reduced error and internal distortion (Table 1). The central sector of both M3C2 displacement models show outliers at the central and southern boundary of the street due to the lack of coherence between the consecutive 3D point clouds after the demolition of the warehouse (Fig. 5). Additionally, the SfM-derived displacement model displays a small area around 1 m^2 with spurious high subsidence rates of up to 38.2 mm/yr (Fig. 5c), which it is not identifiable onsite and should be related to the internal distortion of one of the photogrammetric models. In order to better compare the performance of TLS and close-range SfM photogrammetry for monitoring the investigated sinkhole we have disregarded these non-reliable extreme values from the datasets. A common approach for normal distributions is to calculate their upper and lower bounds. Regarding the subsidence rate values derived from the M3C2 displacement models, the lower bound can be defined as $Q1 - 1.5 * IQR$ (Inter-Quartile Range), that is 17.2 and 15.2 mm/year for the TLS- and the SfM-derived models, respectively. These values are smaller but consistent with the maximum subsidence rate measured by means of high-precision levelling for the same time interval, 22.9 mm/yr,

The comparison of the various deformation rates computed for the same time span along the high-precision leveling line reveals a general underestimation of the subsidence rates derived from the M3C2 displacement models compared to the more accurate rates obtained by high-precision leveling (Fig. 6). Along the western part of the profiles, where the displacement rate is slower, high-precision leveling and TLS recorded comparable subsidence rates, while ground-based SfM photogrammetry provided mostly uplift rates with a fluctuating pattern. The central sectors of the profiles describe a trough-like M3C2 displacement rate profile consistent with the sinkhole location. There, TLS and SfM measured similar rates but up to two times slower than the displacement values recorded by high-precision leveling. In the eastern part of the profiles, high-precision leveling measured negative displacement rates corresponding to the additional subsidence structure detected in the leveling line. Here, TLS recorded negligible fluctuating positive and negative displacement rates without detecting the sinkhole, and SfM measured fast subsidence rates spatially consistent with the sinkhole location but with much higher displacement rates compared to high-precision leveling. Additionally, the easternmost section of the SfM displacement profile displayed outliers spatially coincident with the position of sewerage intakes and which may be related to discrepancies between incidence angles and their related occlusion areas. Overall, SfM provided more inconsistent data throughout the whole profile and given its serrated wavy pattern, the maximum positive and negative rates could be related to photogrammetric model distortion and might be reduced using a denser or an alternative GCPs distribution.

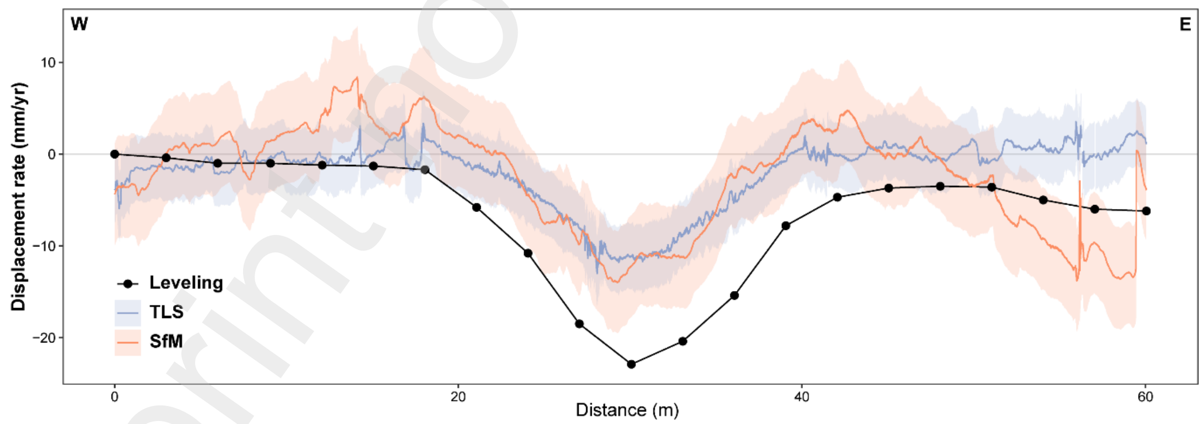

Figure 6. *Displacement rates measured between June 2021 and June 2022 across the S. Lamberto sinkhole with high-precision leveling, TLS, and ground-based SfM photogrammetry. TLS- and SfM-derived M3C2 displacement rates have been gathered along the profile defined by high-precision leveling. The error bands display the mean error of the M3C2 models listed in table 1.*

As shown in this work, TLS- and SfM-derived M3C2 displacement models may significantly underestimate the extent and magnitude of the deformation but provide high-resolution spatially distributed data. Moreover, this areal information, in particular the TLS-derived model (Fig. 5a), has revealed that the high-precision leveling line was not installed across the most rapidly sinking point of the sinkhole and therefore it does not record its maximum subsidence rate. This means that neither the leveling profiles, nor the M3C2 displacement models provided accurate maximum subsiding rates for the S. Lamberto sinkhole, but minimum values. Combining TLS or close-range SfM photogrammetry with a dense network of geodetic benchmarks, including points in the sector of the sinkhole with greatest subsidence, could help reducing the underestimation issues of M3C2 displacement models while providing data with high spatial resolution that high-precision leveling lacks.

Regarding the data-acquisition process, although the capture of the photographs used for photogrammetry in this work required considerable time (manual shooting), its duration can be reduced substantially by taking the images automatically at walking pace using time lapse. This would allow equating the data gathering time of the close-range SfM photogrammetry to the that of the TLS, improving the benefit/effort ratio of the former approach.

Conclusions

This investigation presents for the first time a comparison of the performance of Terrestrial Laser Scanner (TLS) and close-range Structure from Motion (SfM) photogrammetry using a conventional ground-based camera for monitoring a slowly subsiding active sagging sinkhole in an urban area, through the generation of high-resolution Multiscale Model-to-Model Cloud Comparison (M3C2) displacement maps. The displacement models derived from two pairs of 3D point clouds gathered one year apart allowed to detect and measure surface deformation in the most rapidly moving sector of the sinkhole, although underestimating subsidence rates. The TLS-derived M3C2 displacement model provided data with overall less noise and internal distortion, allowing us to identify the extent of the area affected by subsidence and to quantify the deformation rates with greater confidence. However, the more affordable and easier-to-produce SfM-derived M3C2 displacement model supplied comparable data on the extent of the area affected by the sinkhole and subsidence rates.

According to the cumulative vertical deformation profiles constructed with high-precision leveling data, both TLS- and SfM-derived M3C2 displacement models underestimated the extent and subsidence rate of the studied sinkhole. Leveling provided highly accurate and precise quantitative vertical displacement data, including a slow-moving aureole, and served to detect an additional adjoining sinkhole not identified in the geomorphological map produced with conventional data. However, this high-quality information was restricted to the position of the benchmarks and the length of the line, restricted by urban elements, was not long enough to precisely locate the boundary of the S. Lamberto sinkhole.

Close-range SfM photogrammetry, even when implemented with ground-based conventional cameras, can be successfully applied to identify the most rapidly deforming areas of a sinkhole provided that accurate geodetic data (ground control points) are available. It is important to note that at the present time these techniques cannot be used to precisely identify the boundaries of active sinkholes with slow-moving marginal areas. This requires the installation of long high-precision leveling lines extended well beyond the edges of the subsidence areas. The synergistic combination of M3C2 displacement models and high-precision leveling constitute a highly valuable strategy for the comprehensive monitoring of active sinkholes in developed areas.

Data availability

Data will be made available on request

Acknowledgements

The work has been supported by projects CGL2017-85045-P and PID2021-123189NB-I00 of the Spanish Government (Ministerio de Ciencia e Innovación). During data collection and analysis phases, JSA had a pre-doctoral contract (PRE2018-084240) cofinanced by the Spanish Government and the European Social Fund (ESF). FG belongs to the IUCA research group of the Aragón Government.

References

Acero, P., Auqué, L.F., Galve, J.P., Gutiérrez, F., Carbonel, D., Gimeno, M.J., Yechieli, Y., Asta, M.P. and Gómez, J.B. (2015) "Evaluation of geochemical and hydrogeological processes by geochemical modeling in an area affected by evaporite karstification," *Journal of Hydrology*, 529, pp. 1874–1889. https://doi.org/10.1016/j.jhydrol.2015.07.028.

Agisoft PhotoScan Professional (2022). Available at: http://www.agisoft.com/downloads/installer/.

Al-Halbouni, D., AlRabayah, O., Nakath, D. and Rüpke, L. (2022) "A Vision on a UNESCO Global Geopark at the Southeastern Dead Sea in Jordan—How Natural Hazards May Offer Geotourism Opportunities," *Land*, 11(4), p. 553. https://doi.org/10.3390/land11040553.

Al-Halbouni, D., Holohan, E.P., Saberi, L., Alrshdan, H., Sawarieh, A., Closson, D., Walter, T.R. and Dahm, T. (2017) "Sinkholes, subsidence and subrosion on the eastern shore of the Dead Sea as revealed by a close-range photogrammetric survey," *Geomorphology* , 285, pp. 305–324. https://doi.org/10.1016/j.geomorph.2017.02.006.

Anchuela, Ó.P., López, D.A., Juan, A.P., Sainz, A.M.C., Simón, J.L., Gil, H., Lloréns, J.F.I. and Abadías, J.G. (2012) "Consideraciones sobre la construcción en zonas kársticas activas. Caso de la Avenida de las Estrellas de Zaragoza," *Geogaceta*, 51, pp. 63–66. Available at: https://rabida.uhu.es/dspace/bitstream/handle/10272/7291/Consideraciones-sobre.pdf?sequence=2.

Benito-Calvo, A., Gutiérrez, F., Martínez-Fernández, A., Carbonel, D., Karampaglidis, T., Desir, G., Sevil, J., Guerrero, J., Fabregat, I. and García-Arnay, Á. (2018) "4D Monitoring of Active Sinkholes with a Terrestrial Laser Scanner (TLS): A Case Study in the Evaporite Karst of the Ebro Valley, NE Spain," *Remote Sensing*, 10(4), p. 571. https://doi.org/10.3390/rs10040571.

Bezuidenhout, C.A. and Enslin, J.F. (1970) "Surface subsidence and sinkholes in the dolomitic areas of the Far West Rand, Transvaal, Republic of South Africa."

Buchignani, V., Avanzi, G.D., Giannecchini, R. and Puccinelli, A. (2008) "Evaporite karst and sinkholes: a synthesis on the case of Camaiore (Italy)," *Environmental geology*, 53(5), pp. 1037–1044. https://doi.org/10.1007/s00254-007-0730-x.

Buttrick, D.B., Trollip, N.Y.G., Watermeyer, R.B., Pieterse, N.D. and Gerber, A.A. (2011) "A performance based approach to dolomite risk management," *Environmental Earth Sciences*, 64(4), pp. 1127–1138. https://doi.org/10.1007/s12665-011-0929-8.

Carbonel, D., Rodríguez, V., Gutiérrez, F., McCalpin, J.P., Linares, R., Roqué, C., Zarroca, M., Guerrero, J. and Sasowsky, I. (2014) "Evaluation of trenching, ground penetrating radar (GPR) and electrical resistivity tomography (ERT) for sinkhole characterization," *Earth Surface Processes and Landforms*, 39(2), pp. 214–227. https://doi.org/10.1002/esp.3440.

Carbonel, D., Rodríguez-Tribaldos, V., Gutiérrez, F., Galve, J.P., Guerrero, J., Zarroca, M., Roqué, C., Linares, R., McCalpin, J.P. and Acosta, E. (2015) "Investigating a damaging buried sinkhole cluster in an urban area (Zaragoza city, NE Spain) integrating multiple techniques: Geomorphological surveys, DInSAR, DEMs, GPR, ERT, and trenching," *Geomorphology* , 229, pp. 3–16. https://doi.org/10.1016/j.geomorph.2014.02.007.

Chakra, C.A., Gascoin, S., Somma, J., Fanise, P. and Drapeau, L. (2019) “Monitoring the Snowpack Volume in a Sinkhole on Mount Lebanon using Time Lapse Photogrammetry,” *Sensors* , 19(18), p. 3890. https://doi.org/10.3390/s19183890.

CloudCompare (2024). Available at: http://www.cloudcompare.org/.

Daoxian, Y. (1988) “Environmental and engineering problems of karst Geology in China,” *Environmental Geology and Water Sciences*, 12(2), pp. 79–87. https://doi.org/10.1007/BF02574792.

De Waele, J. and Gutierrez, F. (2022) *Karst Hydrogeology, Geomorphology and Caves*. John Wiley & Sons. https://doi.org/10.1002/9781119605379.

Desir, G., Gutiérrez, F., Merino, J., Carbonel, D., Benito-Calvo, A., Guerrero, J. and Fabregat, I. (2018) “Rapid subsidence in damaging sinkholes: Measurement by high-precision leveling and the role of salt dissolution,” *Geomorphology* , 303, pp. 393–409. https://doi.org/10.1016/j.geomorph.2017.12.004.

Dursun, A.E. (2022) “Risk analysis of natural sinkholes hazards in Karapınar basin (Konya, Turkey),” *Arabian Journal of Geosciences*, 15(3), p. 279. https://doi.org/10.1007/s12517-022-09564-8.

FARO SCENE (2023). Available at: https://www.faro.com/es-MX/Products/Software/SCENE-Software.

Galve, J.P., Castañeda, C., Gutiérrez, F. and Herrera, G. (2015) “Assessing sinkhole activity in the Ebro Valley mantled evaporite karst using advanced DInSAR,” *Geomorphology* , 229, pp. 30–44. https://doi.org/10.1016/j.geomorph.2014.07.035.

Galve, J.P., Gutiérrez, F., Lucha, P., Bonachea, J., Remondo, J., Cendrero, A., Gutiérrez, M., Gimeno, M.J., Pardo, G. and Sánchez, J.A. (2009) “Sinkholes in the salt-bearing evaporite karst of the Ebro River valley upstream of Zaragoza city (NE Spain): Geomorphological mapping and analysis as a basis for risk management,” *Geomorphology* , 108(3), pp. 145–158. https://doi.org/10.1016/j.geomorph.2008.12.018.

Goodings, D.J. and Abdulla, W.A. (2002) “Stability charts for predicting sinkholes in weakly cemented sand over karst limestone,” *Engineering Geology*, 65(2), pp. 179–184. https://doi.org/10.1016/S0013-7952(01)00127-2.

Guerrero, J., Gutiérrez, F., Bonachea, J. and Lucha, P. (2008) “A sinkhole susceptibility zonation based on paleokarst analysis along a stretch of the Madrid–Barcelona high-speed railway built over gypsum- and salt-bearing evaporites (NE Spain),” *Engineering Geology*, 102(1), pp. 62–73. https://doi.org/10.1016/j.enggeo.2008.07.010.

Guerrero, J., Sevil, J., Desir, G., Gutiérrez, F., Arnay, Á.G., Galve, J.P. and Reyes-Carmona, C. (2021) “The Detection of Active Sinkholes by Airborne Differential LiDAR DEMs and InSAR Cloud Computing Tools,” *Remote Sensing*, 13(16), p. 3261. https://doi.org/10.3390/rs13163261.

Gutiérrez, F. (2016) “Sinkhole hazards,” in *Oxford Research Encyclopedia of Natural Hazard Science*. Oxford University Press. https://doi.org/10.1093/acrefore/9780199389407.013.40.

Gutiérrez, F., Benito-Calvo, A., Carbonel, D., Desir, G., Sevil, J., Guerrero, J., Martínez-Fernández, A., Karamplaglidis, T., García-Arnay, Á. and Fabregat, I. (2019) "Review on sinkhole monitoring and performance of remediation measures by high-precision leveling and terrestrial laser scanner in the salt karst of the Ebro Valley, Spain," *Engineering Geology*, 248, pp. 283–308. https://doi.org/10.1016/j.enggeo.2018.12.004.

Gutiérrez, F., Calaforra, J.M., Cardona, F., Ortí, F., Durán, J.J. and Garay, P. (2008a) "Geological and environmental implications of the evaporite karst in Spain," *Environmental geology*, 53(5), pp. 951–965. https://doi.org/10.1007/s00254-007-0721-y.

Gutiérrez, F., Galve, J.P., Guerrero, J., Lucha, P., Cendrero, A., Remondo, J., Bonachea, J., Gutiérrez, M. and Sánchez, J.A. (2007) "The origin, typology, spatial distribution and detrimental effects of the sinkholes developed in the alluvial evaporite karst of the Ebro River valley downstream of Zaragoza city (NE Spain)," *Earth Surface Processes and Landforms*, 32(6), pp. 912–928. https://doi.org/10.1002/esp.1456.

Gutiérrez, F., Galve, J.P., Lucha, P., Bonachea, J., Jordá, L. and Jordá, R. (2009) "Investigation of a large collapse sinkhole affecting a multi-storey building by means of geophysics and the trenching technique (Zaragoza city, NE Spain)," *Environmental geology*, 58(5), pp. 1107–1122. https://doi.org/10.1007/s00254-008-1590-8.

Gutiérrez, F., Guerrero, J. and Lucha, P. (2008b) "A genetic classification of sinkholes illustrated from evaporite paleokarst exposures in Spain," *Environmental geology*, 53(5), pp. 993–1006. https://doi.org/10.1007/s00254-007-0727-5.

Gutiérrez, F., Mozafari, M., Carbonel, D., Gómez, R. and Raeisi, E. (2015) "Leakage problems in dams built on evaporites. The case of La Loteta Dam (NE Spain), a reservoir in a large karstic depression generated by interstratal salt dissolution," *Engineering Geology*, 185, pp. 139–154. https://doi.org/10.1016/j.enggeo.2014.12.009.

Gutiérrez, F., Sevil, J. and Migoń, P. (2023a) "Landslides in the Remolinos gypsum escarpment (NE Spain): controls imposed by stratigraphy, fluvial erosion, and interstratal salt dissolution," *Landslides*, 20(10), pp. 2075–2093. https://doi.org/10.1007/s10346-023-02090-y.

Gutiérrez, F., Sevil, J., Sevillano, P., Preciado-Garbayo, J., Martínez, J.J., Martín-López, S. and González-Herráez, M. (2023b) "The application of distributed optical fiber sensors (Botda) to sinkhole monitoring. Review and the case of a damaging sinkhole in the Ebro valley evaporite karst (NE Spain)."

Gutiérrez, F., Zarroca, M., Linares, R., Roqué, C., Carbonel, D., Guerrero, J., McCalpin, J.P., Comas, X. and Cooper, A.H. (2018) "Identifying the boundaries of sinkholes and subsidence areas via trenching and establishing setback distances," *Engineering Geology*, 233, pp. 255–268. https://doi.org/10.1016/j.enggeo.2017.12.015.

ISO 17123-2 (2001). Geneva, Switzerland: Optics and optical instruments Field procedures for testing geodetic and surveying instruments Part 2: Levels.

Jones, C.E. and Blom, R.G. (2014) "Bayou Corne, Louisiana, sinkhole: Precursory deformation measured by radar interferometry," *Geology*, 42(2), pp. 111–114. https://doi.org/10.1130/G34972.1.

Kersten, T., Kobe, M., Gabriel, G., Timmen, L., Schön, S. and Vogel, D. (2017) "Geodetic monitoring of subrosion-induced subsidence processes in urban areas," *Journal of Applied Geodesy*, 11(1), pp. 21–29. https://doi.org/10.1515/jag-2016-0029.

Kobe, M., Gabriel, G., Weise, A. and Vogel, D. (2019) "Time-lapse gravity and levelling surveys reveal mass loss and ongoing subsidence in the urban subrosion-prone area of Bad Frankenhausen, Germany," *Solid earth*, 10(3), pp. 599–619. https://doi.org/10.5194/se-10-599-2019.

Lague, D., Brodu, N. and Leroux, J. (2013) "Accurate 3D comparison of complex topography with terrestrial laser scanner: Application to the Rangitikei canyon (N-Z)," *ISPRS journal of photogrammetry and remote sensing: official publication of the International Society for Photogrammetry and Remote Sensing* , 82, pp. 10–26. https://doi.org/10.1016/j.isprsjprs.2013.04.009.

Lei, M., Jiang, X. and Guan, Z. (2013) "Emergency investigation of extremely large sinkholes, Maohe, Guangxi, China," in L. Land, D.H. Doctor, and J.B. Stephenson (eds.) *Sinkholes and the engineering and environmental impacts of karst*. *Thirteenth Multidisciplinary Conference*, National Cave and Karst Research Institute, pp. 145–151. https://doi.org/10.5038/9780979542275.1139.

Martínez-Fernández, A., Serrano, E., Pisabarro, A., Sánchez-Fernández, M., de Sanjosé, J.J., Gómez-Lende, M., Rangel-de Lázaro, G. and Benito-Calvo, A. (2022) "The Influence of Image Properties on High-Detail SfM Photogrammetric Surveys of Complex Geometric Landforms: The Application of a Consumer-Grade UAV Camera in a Rock Glacier Survey," *Remote Sensing*, 14(15), p. 3528. https://doi.org/10.3390/rs14153528.

Menezes, D.F., Bezerra, F.H., Balsamo, F., Arcari, A., Maia, R.P. and Cazarin, C.L. (2020) "Subsidence rings and fracture pattern around dolines in carbonate platforms – Implications for evolution and petrophysical properties of collapse structures," *Marine and Petroleum Geology*, 113, p. 104113. https://doi.org/10.1016/j.marpetgeo.2019.104113.

Micheletti, N., Chandler, J. and Lane, S.N. (2015) "Structure from motion (SFM) photogrammetry," in Clarke, L.E. and Nield, J.M. (ed.) *Geomorphological Techniques (Online Edition)*. Available at: http://www.geomorphology.org.uk/sites/default/files/geom_tech_chapters/2.2.2_sfm.pdf.

Orhan, O., Haghshenas Haghighi, M., Demir, V., Gökkaya, E., Gutiérrez, F. and Al-Halbouni, D. (2023) "Spatial and Temporal Patterns of Land Subsidence and Sinkhole Occurrence in the Konya Endorheic Basin, Turkey," *Geosciences Journal*, 14(1), p. 5. https://doi.org/10.3390/geosciences14010005.

Parise, M., Closson, D., Gutiérrez, F. and Stevanović, Z. (2015) "Anticipating and managing engineering problems in the complex karst environment," *Environmental Earth Sciences*, 74(12), pp. 7823–7835. https://doi.org/10.1007/s12665-015-4647-5.

Petschko, H., Zehner, M., Fischer, P. and Goetz, J. (2022) "Terrestrial and Airborne Structure from Motion Photogrammetry Applied for Change Detection within a Sinkhole in Thuringia, Germany," *Remote Sensing*, 14(13), p. 3058. https://doi.org/10.3390/rs14133058.

QGIS.org (2023) *QGIS Geographic Information System*. Available at: http://qgis.org.

Quirantes, J. (1978) “Estudio sedimentológico y estratigráfico del terciario continental de los Monegros. Zaragoza, Diputación Provincial de Zaragoza (DPZ),” *Publicaciones de la Institución Fernando el Católico (CSIC), 207pp* [Preprint].

R Core Team (2022) *R: A language and environment for statistical computing. R Foundation for Statistical Computing, Vienna, Austria*. Available at: https://www.R-project.org/.

Salvany, J.M. (2009) *Geología del yacimiento glauberítico de Montes de Torrero*. Prensas de la Universidad de Zaragoza.

Salvany, J.M., García-Veigas, J. and Ortí, F. (2007) “Glauberite-Halite association of the Zaragoza gypsum formation (lower Miocene, Ebro basin, NE Spain),” *Sedimentology*, 54(2), pp. 443–467. https://doi.org/10.1111/j.1365-3091.2006.00844.x.

Sevil, J., Benito-Calvo, A. and Gutiérrez, F. (2021) “Sinkhole subsidence monitoring combining terrestrial laser scanner and high-precision levelling,” *Earth Surface Processes and Landforms*, 46(8), pp. 1431–1444. https://doi.org/10.1002/esp.5112.

Sevil, J., Gutiérrez, F., Carnicer, C., Carbonel, D., Desir, G., García-Arnay, Á. and Guerrero, J. (2020) “Characterizing and monitoring a high-risk sinkhole in an urban area underlain by salt through non-invasive methods: Detailed mapping, high-precision leveling and GPR,” *Engineering Geology*, 272, p. 105641. https://doi.org/10.1016/j.enggeo.2020.105641.

Sevil, J., Gutiérrez, F., Zarroca, M., Desir, G., Carbonel, D., Guerrero, J., Linares, R., Roqué, C. and Fabregat, I. (2017) “Sinkhole investigation in an urban area by trenching in combination with GPR, ERT and high-precision leveling. Mantled evaporite karst of Zaragoza city, NE Spain,” *Engineering Geology*, 231, pp. 9–20. https://doi.org/10.1016/j.enggeo.2017.10.009.

Theron, A., Engelbrecht, J., Kemp, J., Kleynhans, W. and Turnbull, T. (2017) “Detection of Sinkhole Precursors Through SAR Interferometry: Radar and Geological Considerations,” *IEEE Geoscience and Remote Sensing Letters*, 14(6), pp. 871–875. https://doi.org/10.1109/LGRS.2017.2684905.

Vassileva, M., Al-Halbouni, D., Motagh, M., Walter, T.R., Dahm, T. and Wetzel, H.-U. (2021) “A decade-long silent ground subsidence hazard culminating in a metropolitan disaster in Maceió, Brazil,” *Scientific reports*, 11(1), p. 7704. https://doi.org/10.1038/s41598-021-87033-0.

Waltham, A.C., Bell, F.G. and Culshaw, M.G. (2005) *Sinkholes and Subsidence*. Springer Berlin Heidelberg. https://doi.org/10.1007/b138363.

Westoby, M.J., Brasington, J., Glasser, N.F., Hambrey, M.J. and Reynolds, J.M. (2012) “‘Structure-from-Motion’ photogrammetry: A low-cost, effective tool for geoscience applications,” *Geomorphology* , 179, pp. 300–314. https://doi.org/10.1016/j.geomorph.2012.08.021.

Zhang, Z. (1994) “Iterative point matching for registration of free-form curves and surfaces,” *International journal of computer vision*, 13(2), pp. 119–152. https://doi.org/10.1007/BF01427149.

Zini, L., Calligaris, C., Forte, E., Petronio, L., Zavagno, E., Boccali, C. and Cucchi, F. (2015) "A multidisciplinary approach in sinkhole analysis: The Quinis village case study (NE-Italy)," *Engineering Geology*, 197, pp. 132–144. https://doi.org/10.1016/j.enggeo.2015.07.004.